Science of the Total Environment 699 (2020) 134381

Contents lists available at ScienceDirect

Science of the Total Environment

journal homepage: www.elsevier.com/locate/scitotenv

Impacts of temperature on evolution of char structure during pyrolysis of lignin

Chenting Zhang [a], Yuewen Shao [a], Lijun Zhang [a], Shu Zhang [b], Roel J.M. Westerhof [c], Qing Liu [d], Peng Jia [a], Qingyin Li [a], Yi Wang [e,*], Xun Hu [a,*]

[a] School of Material Science and Engineering, University of Jinan, Jinan, 250022, PR China
[b] College of Materials Science and Engineering, Nanjing Forestry University, 210037, Nanjing, PR China
[c] Sustainable Process Technology Group, University of Twente, Enschede, 7522, the Netherlands
[d] Key Laboratory of Low Carbon Energy and Chemical Engineering, College of Chemical and Environmental Engineering, Shandong University of Science and Technology, Qingdao 266590, Shandong, PR China
[e] School of Energy and Power Engineering, Huazhong University of Science and Technology, Wuhan, 430074, PR China.

HIGHLIGHTS

- C/H ratio in different char is equivalent to that in fused rings of varied size.
- Increasing pyrolysis temperature shifted ketones, esters in bio-oil to ethers.
- Tar obtained above 550 °C had a higher oxygen content but better thermal stability.
- DRIFTS study shows the drastic structural changes of char occurred at 520 to 530 °C.

GRAPHICAL ABSTRACT

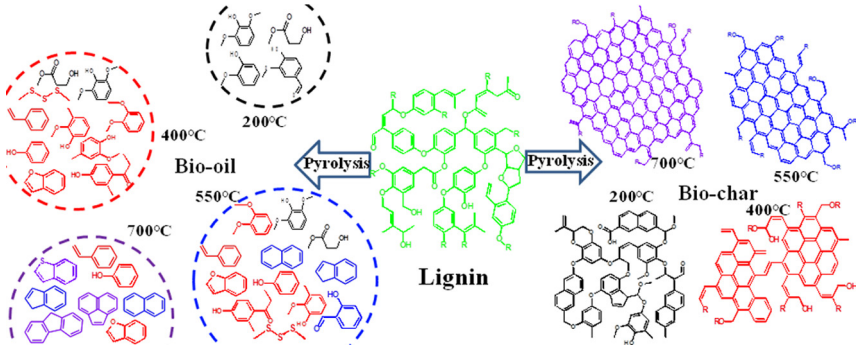

ARTICLE INFO

Article history:
Received 28 June 2019
Received in revised form 3 September 2019
Accepted 8 September 2019
Available online 10 September 2019

Editor: Daniel CW Tsang

Keywords:
Pyrolysis of lignin
Impacts of temperature
Structure of char
DRIFTS study of pyrolysis

ABSTRACT

This study investigated the pyrolysis of lignin pyrolysis in a temperature region from 200 to 800 °C, aiming to understand influence of pyrolysis temperature on evolution of structures of the resulting char. The results showed that fusion of the ring structure initiated at 200 °C, where the C/H ratio in the char was equal to that in naphthalene (two fused rings). The C/H ratio in the char obtained at 350 °C corresponded to that in pyrene (four fused rings), while the char produced at 550 °C was equivalent to 20 fused benzene rings in terms of C/H ratio. The increasing pyrolysis temperature also shifted the oxygen-containing functionalities such as the carbonyl, esters, ketones in the bio-oil to the ether functionality that had a higher thermal stability. The DRIFTS study of pyrolysis of lignin showed that drastic changes of the functionalities and the internal structure of the char occurred in a narrow temperature region from 520 to 530 °C. The carbonyl functionality and the aliphatic structure were eliminated, and new conjugated π-bond systems formed.

* Corresponding authors.
E-mail addresses: alenwang@hust.edu.cn (Y. Wang), xun.hu@outlook.com (X. Hu).

https://doi.org/10.1016/j.scitotenv.2019.134381
0048-9697/

1. Introduction

Biomass is carbon-neutral and widely distributed, which is a renewable source of energy, chemicals and fuels. Via pyrolysis, biomass can be converted into gaseous products, the liquid product named as bio-oil and the solid product named as biochar (Kan et al., 2016; Buller et al., 2015; Han et al., 2019). The main characteristics of bio-oil and biochar are the complexity in terms of composition or structure. This is due to the complicated reaction network during the pyrolysis of biomass, which again originates from the complexity of biomass (Chan et al., 2019; Chen et al., 2018; Hu and Gholizadeh, 2019).

Woody biomass is typically composed by three different components, namely cellulose, hemicellulose and lignin. The ratio of these three components in different biomass species or even different parts of the same biomass source is different (Abhishek et al., 2015; Gholizadeh et al., 2019). When the biomass is pyrolyzed, these components could be pyrolysed in parallel, making the pyrolysis process to become a complex reaction network (Chaiwat et al., 2013; Stefanidis et al., 2014). Understanding the reaction pathways of the subcomponents of biomass is critical for optimizing the parameters for pyrolysis for production of the bio-oil with desirable compositions or the biochar with desirable structures (José et al., 2019; Das et al., 2015).

The bio-oil with tailored composition is of importance for its directly utilization or further upgrading via hydrotreatment, while the biochar with tailored structure is also crucial for the use as functional carbon materials for various uses such as activated carbon, electrode materials, etc. (Iliopoulou et al., 2014; Xiong et al., 2017; Hoslett et al., 2019). Lignin is an important fraction of biomass and its pyrolysis has been widely investigated (Gunawan et al., 2013; Dhyani and Bhaskar, 2018; Sharma et al., 2004; Wang et al., 2017; Zhao et al., 2017; Ma et al., 2019). Research on the pyrolysis characteristics of lignin is mainly divided into two categories. The first category is the pyrolysis analysis of lignin from different biomass or extracted by different methods. The second is the pyrolysis study of model compounds of lignin. The physicochemical properties, pyrolysis kinetics and product distribution and composition of lignin were described in these previous literatures. However, due to the complex structure and pyrolysis reaction network system of lignin, the reaction mechanism of lignin pyrolysis has not been fully understood (Ha et al., 2019). Understanding the pyrolysis mechanism of lignin can help to tailor the selectivity of the targeting products and explore the causes of catalyst deactivation during catalytic pyrolysis. In this work, in addition to analyzing the pyrolysis kinetics of lignin and the characteristics of the products generated by lignin pyrolysis, the in-situ DRIFTS analysis of the evolution of the functionalities during pyrolysis of lignin was conducted to explore the pyrolysis mechanism of lignin. We have to admit that to the current results of this study we have not fully clarified the mechanism, but this study, especially the in-situ DRIFTS characterization of the change of the functionalities of lignin versus increasing pyrolysis temperature as well as the detailed characterization of the char produced at the different temperatures, are new additions to understand the mechanism for pyrolysis of lignin or the properties of the resulting bio-char generated at the varied temperature.

The pyrolysis of lignin is affected by many factors such as reaction temperature, reaction time, reaction atmosphere, reactor configuration, particle size of raw materials, etc. (Jiang et al., 2010a; Xiong et al., 2018; Zhao et al., 2018). Among them, the reaction temperature is one of the most important factors impacting the pyrolysis of lignin. This is because that in lignin there are many functionalities with varied dissociation energy (Chua et al., 2017). Thus, the temperature affects the sequences in breaking the chemical bonds and further determines the composition of bio-oil and the structure of bio-char (Xiao and Yang, 2013; Gholizadeh et al., 2016).

In this study, we made an effort to investigate the pyrolysis of lignin in a wide temperature range of 200–800 °C with 50 °C increment of each pyrolysis temperature. In total, 13 pyrolysis temperatures were selected and the impacts of the varied pyrolysis temperature on the composition of the resulting bio-oil and the structure of biochar were investigated in a detailed manner. Specially, the formation of the fused ring structures in the biochar was explored and the changes of the functionality of lignin/biochar versus temperature were investigated with an in-situ Diffuse Reflectance Infrared Fourier transform spectroscopy. In addition, the pyrolysis kinetic parameters of lignin and char obtained from the pyrolysis of lignin at 200 °C were calculated via the method of Kissinger.

2. Experimental

2.1. Feedstock preparation

The dealkaline lignin from Tokyo Chemical Industry was used in the study as the raw feedstock. In preparation for the experiment, the sample was dried in static air at 50 °C for 8 h to remove the free moisture. The weight loss of biomass feedstock was about 18 wt% after the drying and the samples were then used directly without any further pretreatment.

2.2. Pyrolysis experiment

The lignin pyrolysis experiment was carried out in a quartz reactor with an inner diameter of 40 mm. Nitrogen with a flow rate of 100 mL/min was used as a flush gas and also carrier gas to purge the reactor so as to ensure the inert atmosphere of the pyrolysis. When the temperature of the pyrolysis zone reached the required temperature and stabilized, a quartz tube loaded with 5 g of lignin was pushed into the pyrolysis zone for the occurrence of the pyrolysis. The volatiles generated during the pyrolysis were carried away by N_2 and were trapped into four condensing tubes connected in series and cooled in a mixture of icy water. The mixture of methanol and chloroform with a volumetric ratio of 1:4 and a total volume of 10 mL was used as the absorbent. The abundance of the incondensable gases was continuously measured with online gas detectors from the very start of the pyrolysis experiments.

At end of the experiment, all the absorbents in the four condensate tubes were collected and mixed. The mixture of the absorbent and the bio-oil was placed at 35 °C for 4 h resulted in the evaporation of light components of the bio-oil. The yield of remaining heavy bio-oil named as the tar can be obtained by weighing and calculating, which follows the procedures detailed in our previous work (Zhang et al., 2018). For the accuracy of the experiment, the measurement of each sample was repeated for three times to guarantee the accuracy of the experiment experimental error in the yield measurements should be within ±1.5%.

2.3. Analysis methods

Elemental analysis (EA) was performed to analyze the contents of C, N, H, O and S in the feedstock, tar and char by using EuroEA3000-Single instrument. Shimadzu GC–MS (GCMS–QP2020) was used to measure the light component of bio-oil in both qualitative and quantitative ways. The detailed parameters of GC–MS during the measuring process can refer to our previous work (Zhang et al., 2018). The identification of organic molecules in the bio-oils was accomplished by matching the data in the NIST library. Quantitative analysis was performed by the external

standard method via injection of the reference chemicals. For the compounds without reference chemicals available, the peak areas were normalized for comparison of the abundance on one basis.

UV-fluorescence spectroscopy characterization was performed to investigate the relative abundance of the compounds with fused π-bond structures in bio-oil by using Shimadzu RF–6000. The molecular structure of the components in bio-oil was explored by using the Ultraviolet spectrophotometer (Metash Corp, UV-800S). The distribution of functional groups in the tar and char was measured with the Fourier Transform infrared (FT-IR) spectroscopy instrument (Nicolet iS50).

Thermogravimetric (TG) analysis was used to explore the thermal stability of char and tar using the HCT–1 (Henven) instrument. During the heating process, the gaseous products generated via thermal decomposition were fed into an in–situ mass spectrometer (Pfeiffer, MS GSD 320) for analyzing the content of the gaseous composition (CO, CO_2, H_2, CH_4 and C_2H_4) in the exhaust gas. In addition, for getting kinetic parameters of lignin and char from TG experiments, about 10 mg of sample was heated from room temperature to 700 °C at different heating rate (10, 20, 30 and 40 °C/min) in the N_2 atmosphere.

Diffuse Reflectance Infrared Fourier transform spectroscopy (DRIFTS) can measure the evolution of the functional groups in char with temperatures by using the Nicolet IS50 instrument equipped with a modified Harrick Praying Mantis DRIFTS cell. Temperature programmed oxidation (TPO, PCA–1200) technique was used to explore the reactivity of char. X-ray diffraction (XRD) was performed to explore the crystal phase structure of char by using Ultima IV X-ray. FT-Raman spectroscopy (Horiba LabRam HR Evolution instrument) was used to investigate the aromatic hydrocarbon systems in char.

2.4. Pyrolysis kinetic parameters

In order to explore the difference in pyrolysis characteristics between char and lignin, the kinetics of char and lignin had been studied. Although the experimental data and the calculated data can be well fit by the distributed activation energy model. However, due to its empirical nature, the model cannot discuss the kinetic parameters from the perspective of the reaction mechanism (Shuping et al., 2010; Jiang et al., 2012). Therefore, as a method for calculating kinetic parameters, the Kissinger's method was used to explain the thermal decomposition by calculating a series of important parameters (Anca-Couce et al., 2014), such as activation energy, indicating pre-factor, reaction series, etc.

The Eq. (1) can be used to simulate the decomposition rate of solid materials. The reaction order of the solid material can be used to define by n. The reaction rate can be expressed as the rate of consumption of the solid material.

$$\frac{d\alpha}{dt} = k(1-\alpha)^n \tag{1}$$

where α represents the degree of decomposition of solid materials, as expressed in Eq. (2). The k is the rate constant given by the Eq. (3).

$$\alpha = \frac{m_0 - m}{m_0 - m_\infty} \tag{2}$$

where M is the original weight before the reaction, while m_∞ is the final mass after the reaction, the m is the mass at time.

$$k = A\exp\left(\frac{-E_a}{RT}\right) \tag{3}$$

where frequency factor is represented by A, E express the activation energy and T is the reaction temperature (K). Substitution of Eq. (3) into Eq. (1) yields:

$$\frac{d\alpha}{dt} = A\exp\left(\frac{-E_a}{RT}\right)(1-\alpha)^n \tag{4}$$

For a linear heating rate, β = dT/dt, Eq. (4) changes into:

$$\frac{d\alpha}{dT} = \frac{A}{\beta}\exp\left(\frac{-E_a}{RT}\right)(1-\alpha)^n \tag{5}$$

The kinetic parameters A, E and n in this study could be obtained by the method of Kissinger. This method is based on multi-heating rates to calculate the activation energy via the maximum reaction temperature and order of reaction by using the shape of the mass loss-time curve (Kissinger, 1957). With the increasing reaction temperature, the reaction rate dα/dt would rise to a maximum value. At this point, the temperature at which the maximum reaction rate is reached is defined as T_M. Activation energy E can be derived from the slope of $\ln(\beta/T_M^2)$ against $1/T_M$ (=−E/R). The reaction order can be obtained by Eq. (6).

$$S = 0.63n^2 \tag{6}$$

In general, the high value of n indicates the high degree of symmetry of curve. The DTG curve can be used to determine the value of S. Furthermore, the absolute value of the slope on both sides of the curve inflection point can quantitatively describe the peak shape.

$$S = \left|\frac{\left(d^2\alpha/dT^2\right)_L}{\left(d^2\alpha/dT^2\right)_R}\right| \tag{7}$$

According to the value of n and E_a, the value of A can be deduced according to Eq. (5).

3. Results and discussion

3.1. The overall yields of the pyrolysis product

The yields of liquid, solid and gaseous products produced by pyrolysis of lignin at the different reaction temperatures were shown in Fig. 1. Reaction temperature had a substantial influence on distribution of the products. In general, the increase of reaction temperature shifted the main products from char to bio-oil and then to gases. The pyrolysis could be roughly divided into four stages. The temperature below 300 °C was the initial stage of pyrolysis. Not much gaseous products and bio-oil were produced at this stage while the mass of the solid products (char) reduced remarkably. The dealkaline lignin used contained abundant sulfonic acid groups, the removal of which was one reason responsible for the weight decrease. Another reason was the initiation of the pyrolysis and the re-arrangement of the structure, which will be discussed later.

The pyrolysis temperature of 300 to 450 °C could be defined as the second stage of pyrolysis, where the pyrolysis degree of lignin began to intensify. The yield of char decreased significantly from 72.5 to 58.0%. Simultaneously, the yield of tar and gaseous products increased correspondingly. CO_2 and CH_4 were formed from 300 °C, while CO was formed at 350 °C. Lignin contained abundant oxygen-containing functionalities such as carboxyl group, methoxyl group, carbonyl group and hydroxyl group. The carboxyl group had low thermal stability and thus can be removed by heat to form CO_2 (Collard and Blin, 2014). Methane may be formed by $^*CH_3$ via breaking of alkane bonds and the recombination with $^*H$. CO might have been evolved from the cracking of carbonyl group or —COH in lignin. The cracking of these functionalities also led to the formation of more tar and the maximum was achieved at 450 °C.

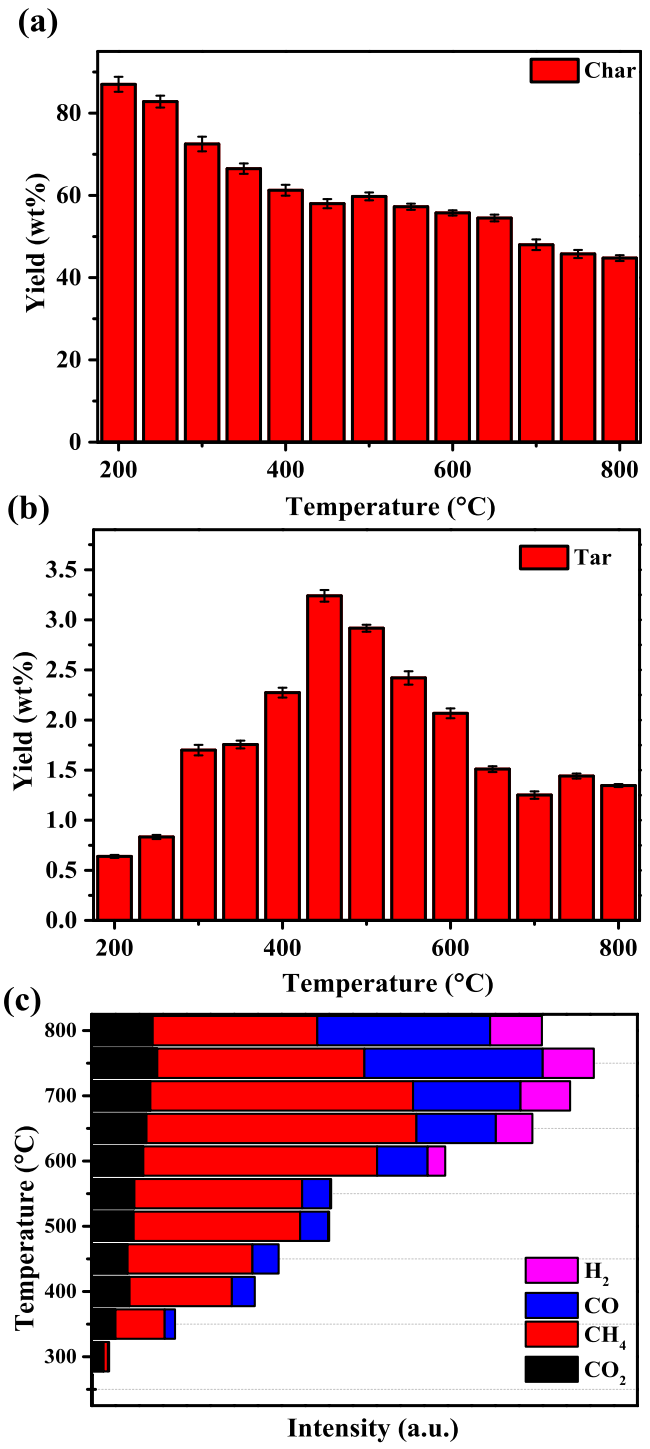

Fig. 1. The char, tar and gas contents from cellulose under different reaction temperature in the pyrolysis: (a) char; (b) tar; (c) gas. (The yields of char or tar = the mass of char or tar / the mass of the raw material × 100%). Reaction conditions: Pyrolysis time = 30 min; P = 1 atm; flow rate of nitrogen = 100 mL/min; Feedstock = 5 g.

The third stage was from 500 to 700 °C. The yield of char was basically stable, while the yield of tar gradually decreased. The gaseous products start to dominate. The production of hydrogen above 600 °C indicated the occurrence of dehydrogenation reactions, or the formation of the fused ring reactions. From 700 °C, the distribution of the main pyrolysis products did not change much, which can be termed as the fourth stage. The main reaction at this stage was the re-construction of the structure of biochar, which will be discussed later. At the varied stages/temperatures, not only the yields but also the compositions/structures of the main pyrolysis products were different, which were further investigated.

3.2. On-line gas analysis

The formation of the gaseous products generated by the pyrolysis at the varied reaction temperature versus reaction time was shown in Fig. 2. Appreciable amount of gases was only formed at 300 °C and became obvious at 350 °C. CO, CO_2 and CH_4 were dominated in the gaseous mixture and CO was formed earlier than CO_2. Above 600 °C, the presence of H_2 indicated the substantial occurrence of dehydrogenation reactions. In addition, the time for the formation of the gaseous products initiated earlier at the higher temperatures than at the lower temperatures, due to the heat transfer limitations. However, the patterns for the distribution of the gases such as CO differed at the high temperatures from that at the lower temperatures. At the low pyrolysis temperature, the formation of CO increased first and then decreased, while the tendency for CO production at the pyrolysis temperature above 700 °C was more complex. In the pyrolysis process, the curve of CO gas versus reaction time showed two peaks. This may be the result of the reverse water gas reaction that converts CO_2 and H_2 to CO at the high temperature. In the other hand, the CO concentration might also be affected by the gasification of the char structure with the CO_2. These two reactions also explain that the abundance of CO_2 gas decreased at the high temperatures.

3.3. Elemental composition of product

The elemental composition of C, H, O and S in char and tar formed from the lignin pyrolysis at the different temperatures was listed in Tables 1 and 2, respectively. In order to better describe the change trend of C, H, O and S with pyrolysis temperature, arranged into the Fig. S1. In addition, the Fig. S1 also depicted graphically the C/H ratio and C/O ratio in char and tar. Below 300 °C, the desulfurization reaction occurred, accompanied by some dehydration reactions. It needs to note that the elemental composition of char obtained at 200 °C was very different from that of the dealkaline lignin. The carbon content significantly increased, while the oxygen content and the sulfur content were correspondingly reduced, which was due to the loss of sulfonic groups that contains not only sulfur but also oxygen.

The increase of temperature increased the C/H ratio, indicating that the structure of char was more aromatic. At 200 °C, the C/H ratio in the char was only 1.2, which was closed to that of naphthalene. When the temperature rose to 350 °C, the C/H ratio was comparable to that of pyrene. At 500 °C, the C/H ratio was equivalent to that of 20 benzene rings, and at 700 °C, the C/H ratio increased to the maximum. Nevertheless, with the further increase of temperature to 800 °C, the C/H ratio decreased to some extent, which was possibly induced by the gasification or cracking of some ring structures. In addition, the increase of the carbon content while the decrease of the oxygen content followed almost similar rhythm.

As also depicted in Fig. S3c, the change of carbon and oxygen contents could be roughly categorized into stage of I of 200–250 °C, stage of II of 300–450 °C, stage of III of 500–700 °C, stage of IV of 750–800 °C, which corresponded to the different reaction network of the pyrolysis at the varied temperatures. Table 2 shows the elemental content of the tar produced at the varied temperature. It needs to note that the tar refers to the residual (heavy bio-oil) after the evaporation of the mixture of bio-oil and absorbing liquid at 35 °C for 4 h. For the tar produced from 300 to 550 °C, the C content was roughly 52%, while the C/H ratio was roughly 0.66. The tar had some extent of unsaturation when compared with glucose that has a carbon content of 40% and a C/H ratio

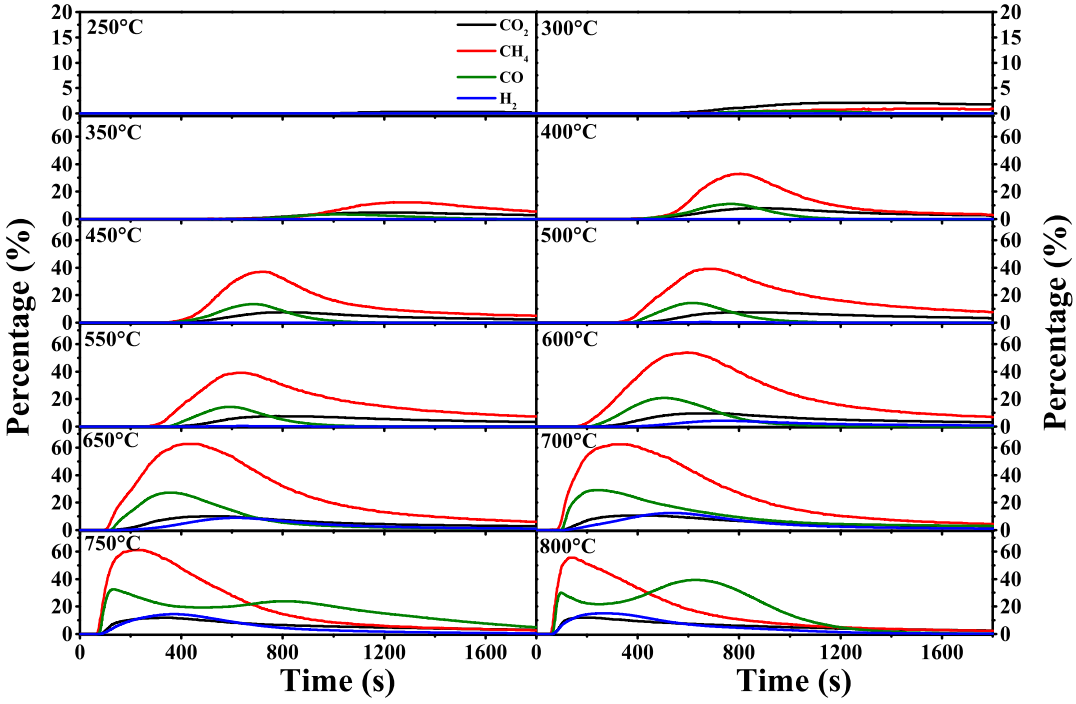

Fig. 2. The gas produced by pyrolysis of lignin at different reaction temperatures changes with time.

Table 1
Element distribution in char produced by lignin biomass pyrolysis at different pyrolysis temperatures[a].

Species	Mass% organic basis				C/O ratio	C/H ratio
	C	H	O	S		
Feedstock						
Lignin	48.3	5.1	40.2	6.4	1.6	0.79
Char						
200 °C	70.6	4.8	21.8	2.8	4.3	1.2
250 °C	73.4	4.9	20.3	1.4	4.8	1.2
300 °C	78.2	4.9	15.9	1.0	6.6	1.3
350 °C	77.4	3.9	18.7	–	5.5	1.7
400 °C	80.7	3.6	15.7	–	6.9	1.9
450 °C	82.0	2.8	15.2	–	7.2	2.4
500 °C	86.4	2.8	10.8	–	10.7	2.6
550 °C	88.4	2.3	9.3	–	12.7	3.2
600 °C	88.9	1.8	9.3	–	12.7	4.1
650 °C	88.3	1.6	10.1	–	11.7	4.6
700 °C	88.8	1.3	9.9	–	12.0	5.7
750 °C	90.8	2.0	7.2	–	16.8	3.8
800 °C	92.0	2.0	6.0	–	20.4	3.8

[a] No nitrogen was detected in the elemental analysis.

of 0.5. Nevertheless, for the tar produced above 550 °C, the carbon content decreased remarkably while, correspondingly, the oxygen content increased remarkably. The deoxygenation of the char transferred the oxygen to the tar and made the tar more oxygen-rich.

3.4. Analysis of bio-oil

3.4.1. GC–MS analysis

Figs. 3 and S2 show the normalized abundance of the light components in the bio-oil produced at the different temperatures, while the actual yield of typical compounds was summarized in Table S1. The phenolics and aromatic hydrocarbons were the main components of the bio-oil, and their distribution and abundance changed substantially with the increase of pyrolysis temperature. At 200 °C, pyrolysis of lignin began to occur, and the ether bond of the linking unit was broken, resulting in the formation of guaiacol and its derivatives (Shen et al., 2014). As the temperature increased, the degree of pyrolysis of the lignin chains intensified, and the abundance of the phenolics like guaiacol reached the maximum at 450 °C.

As the temperatures continued to increase, the phenolics decomposed or condensed with other reactive intermediates, leading to their decreased abundance in the bio-oil (Fig. 3a and b). The simple phenolics like phenol and 4-methylphenol can be produced from the cracking of the phenolic monomers with multiple oxygen-containing functionalities, pyrolytic lignin, etc. Their abundance increased with the increasing pyrolysis temperature. In addition, as shown in Fig. 3b, the phenolics with the carbonyl functionality generally have a lower abundance at the high pyrolysis temperatures. They were probably more reactive to the condensation reactions during the pyrolysis. For the aromatic hydrocarbons such as styrene, they can be formed at the temperature as low as

Table 2
Element distribution in tar produced by lignin biomass pyrolysis at different pyrolysis temperatures[a].

Species	Mass% organic basis				C/O ratio	C/H ratio
	C	H	O	S		
Feedstock						
Lignin	48.3	5.1	40.2	6.4	1.6	0.79
Tar						
300 °C	51.7	6.5	41.8	–	1.6	0.66
350 °C	52.4	6.8	40.8	–	1.7	0.64
400 °C	52.8	6.7	40.5	–	1.7	0.66
450 °C	51.9	6.8	41.3	–	1.6	0.64
500 °C	52.6	6.4	41.0	–	1.7	0.68
550 °C	51.0	6.2	42.8	–	1.5	0.69
600 °C	44.9	5.9	49.2	–	1.2	0.63
650 °C	39.0	5.7	55.3	–	0.94	0.57
700 °C	37.3	5.4	57.3	–	0.87	0.58
750 °C	39.0	5.6	55.4	–	0.94	0.58
800 °C	38.3	5.8	55.9	–	0.91	0.55

[a] No nitrogen was detected in the elemental analysis.

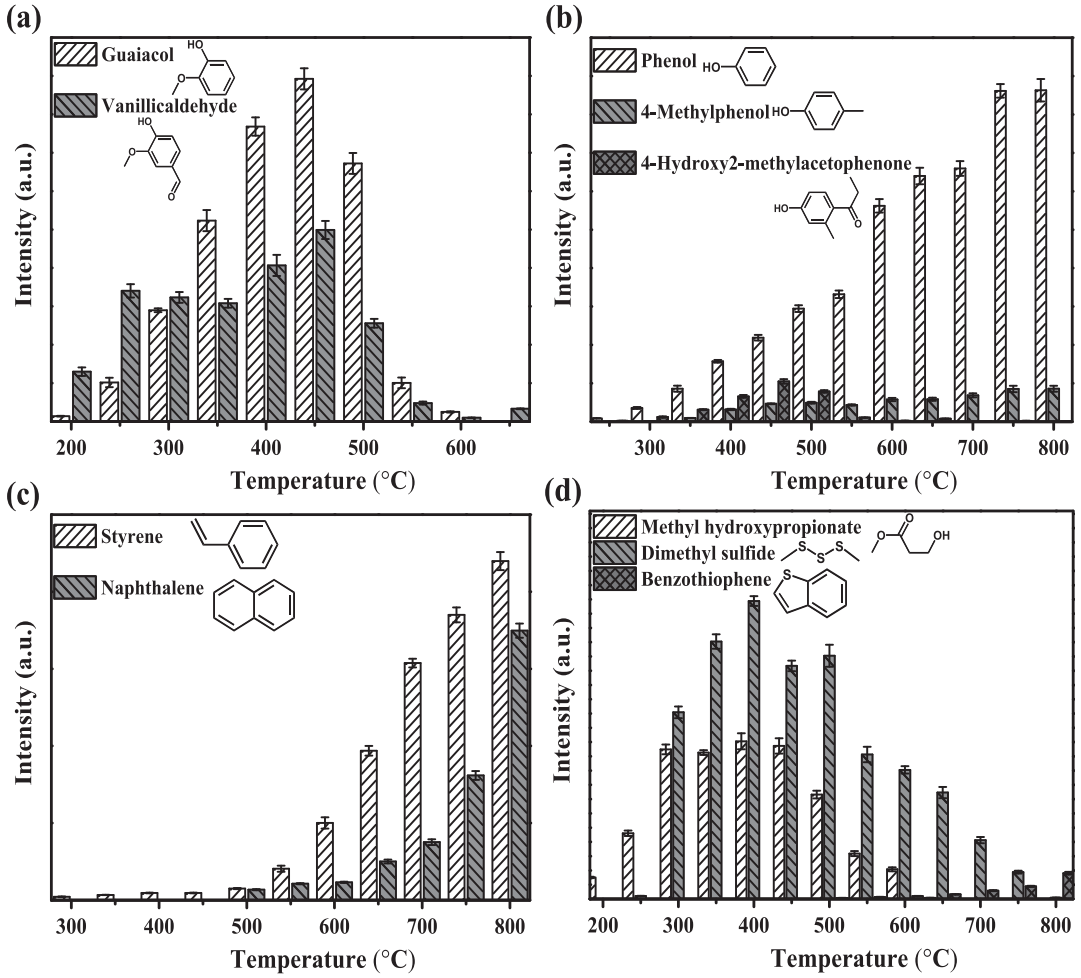

Fig. 3. The composition distribution ofbio-oil from lignin pyrolysis was detected by GSMC.

300 °C. Naphthalene, which has two fused rings, could be formed at least at 500 °C. The increase of reaction temperature promoted their formation via deoxygenation of the phenolics and the fusion of the rings. Some sulfur-containing organics such as benzothiophene were also produced (Fig. 3d), resulting from the decomposition of the sulfur functionality and the subsequent radical reactions for the combination of sulfur with the aromatics. Methyl hydroxypropionate, an aliphatic molecule, was produced from the cracking of the phenolics.

Since GC–MS could only reflect the composition of light components in the bio-oil, the influence of pyrolysis temperature on the generated of the π-conjugated structures in the heavy components was further investigated by UV fluorescence and UV–vis spectroscopy.

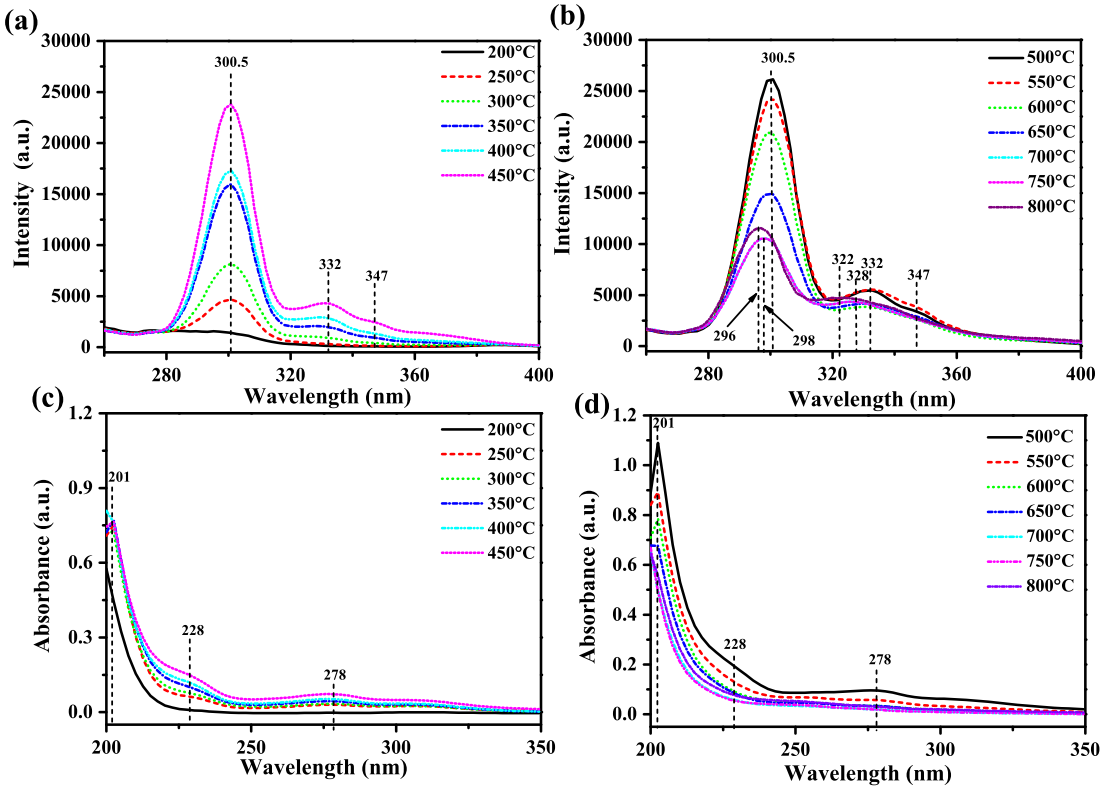

Fig. 4. Fluorescence synchronous spectra (a, b) and ultraviolet spectra (c, d) for the bio-oil from lignin pyrolysis at the different temperature in the pyrolysis.

3.4.2. Analysis of the bio-oils with UV fluorescence and UV–vis spectroscopy

Fig. 4 showed the fluorescence spectra of the bio-oil produced at the varied temperatures. The fluorescence spectra mainly showed the wavelength ranged from 260 to 400 nm, corresponding to the compounds having different aromatic ring structures (Jiang et al., 2016; Wang et al., 2013). For bio-oil produced at 200 °C, there was a weak fluorescent peak at 300.5 nm, assigning to the components with a single aromatic ring, as confirmed with the fluorescence spectra of model compounds (Fig. S3). At 250 °C, the intensity of the fluorescent peak increased, while at 300 °C, new fluorescent peaks appeared at 332 and 347 nm, respectively. The aromatics with two or more fused aromatic rings were formed. The intensity of the fluorescent peaks increased continuously and reached the maximum at 500 °C, while the yield of tar reached the maximum at 450 °C (Fig. 4a). However, above 500 °C, the intensity of the fluorescent peak decreased, and the main peak shifted from 300.5 to 298 nm and then to 296 nm. The shoulder peak shifted from 332 to 328 nm and then to 322 nm. The occurrence of gasification at the elevated temperatures led to the formation of the less amounts of phenolics in the bio-oil, which was in line with the results shown in Table 2, where the carbon content decreased in the tar produced at the high temperatures.

Fig. 4c and d showed the UV–Vis spectroscopy of the bio-oil. For the bio-oil produced 200 °C, only one absorption peak was observed in the range from 200 to 350 nm, which was the E2 band generated by the $\pi \rightarrow \pi^*$ transition in the benzene ring system (Lu et al., 2011; Yin et al., 2010). When the pyrolysis temperature rose to 250 °C, two weak absorption peaks appeared at 220–245 nm and 260–280 nm, which were attributed to the B-band generated by the $\pi \rightarrow \pi^*$ transition and the R-band generated by the $n \rightarrow \pi^*$ transition. The R band was attributed to the phenolics with carbonyl functionalities (Kim et al., 2012; Rover and Brown, 2013). Moreover, under the combined effects of the benzene ring and the carbonyl group, the absorption of the R band and the B band showed a red shift and the intensity was enhanced. The absorbance of the three bands hit a maximum as the pyrolysis temperature reached 500 °C. The further increase of the temperature, however, decreased the intensity of the absorption while the R band was not detected in the spectrum of the bio-oil produced at 700 °C, The GC–MS results also showed that the aldehydes, ketones or esters could not be detected at this high temperature (Fig. 4d). In addition, the tar (the heavy fraction of bio-oil) was further studied with FT-IR and TG-MS.

3.5. Analysis of the tar

3.5.1. FT–IR characterization of the tar

Fig. 5 shows the FT-IR spectra of the tar generated at the different pyrolysis temperatures. The absorption patterns for the bio-oil show some similarities. The peak at 3360 cm^{-1} belonged to the absorption peak of the hydroxyl group in phenols or water. The absorption peaks at 2960, 2920 and 2850 cm^{-1} were the C—H stretching vibration of saturated alkanes. The absorption peaks in the range of 1850–1560 cm^{-1} were complex, and were divided into 7 Gaussian bands by deconvolution, as shown in Fig. 5c to g. The absorption peaks at 1768, 1745, 1710, 1673 and 1593 cm^{-1} corresponded to lactones, esters, aromatic aldehydes/acids, aromatic ketones and alkene, respectively (Lievens et al., 2011). Fig. 5h showed the changes of the abundance of the above five peaks at the different pyrolysis temperatures. With the increase of pyrolysis temperature, the abundance of esters, aromatic aldehydes/acids, aromatic ketones and alkene increased correspondingly until 500 °C. Above this temperature, their absorbance decreased correspondingly, as pyrolysis of lignin pyrolysis tended to produce more gaseous products at this stage. The absorption peaks of benzene ring skeleton vibration at 1510 and 1469 cm^{-1} also showed similar changes. However, as the pyrolysis temperature increased, the

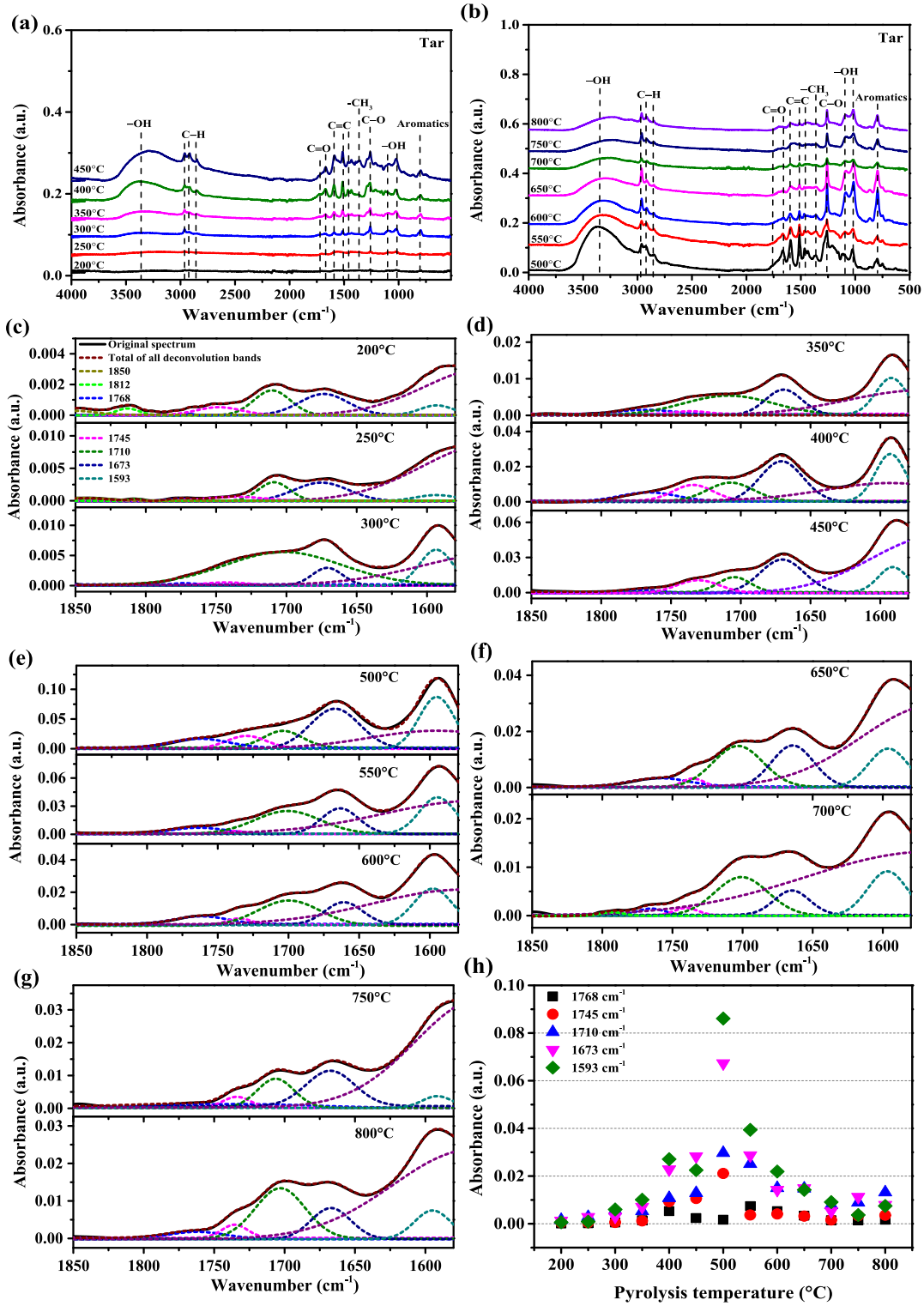

Fig. 5. (a,b) FT–IR characterization of bio-oil from lignin pyrolysis at different recation temperature; (c–g) The absorption peak of FT-IR spectra in the range from 1850 to 1560 cm^{-1} was obtained by deconvolution; (h) The absorbance of Gaussian bands at different pyrolysis temperature.

number of branched chains on the benzene ring decreased, leading to an increase in the absorption of C—H bonds. In addition, the absorption peak of —OH at 1100 and 1020 cm^{-1} and =C—H at 800 cm^{-1} also greatly increased after 550 °C. In the spectra, the ether bond corresponded to the absorption peak at 1260 cm^{-1}, which had a higher thermal stability than the oxygen-containing groups such as aldehyde group or carbonyl group. Nevertheless, after increasing the pyrolysis temperature to 700 °C, the absorbance of each peaks were drastically reduced due to the substantial decrease in the yield of tar.

3.5.2. TG-MS characterization

The TG-MS characterization results of the tar produced at the typical temperature of 300, 400, 500 and 650 °C in N_2 was shown

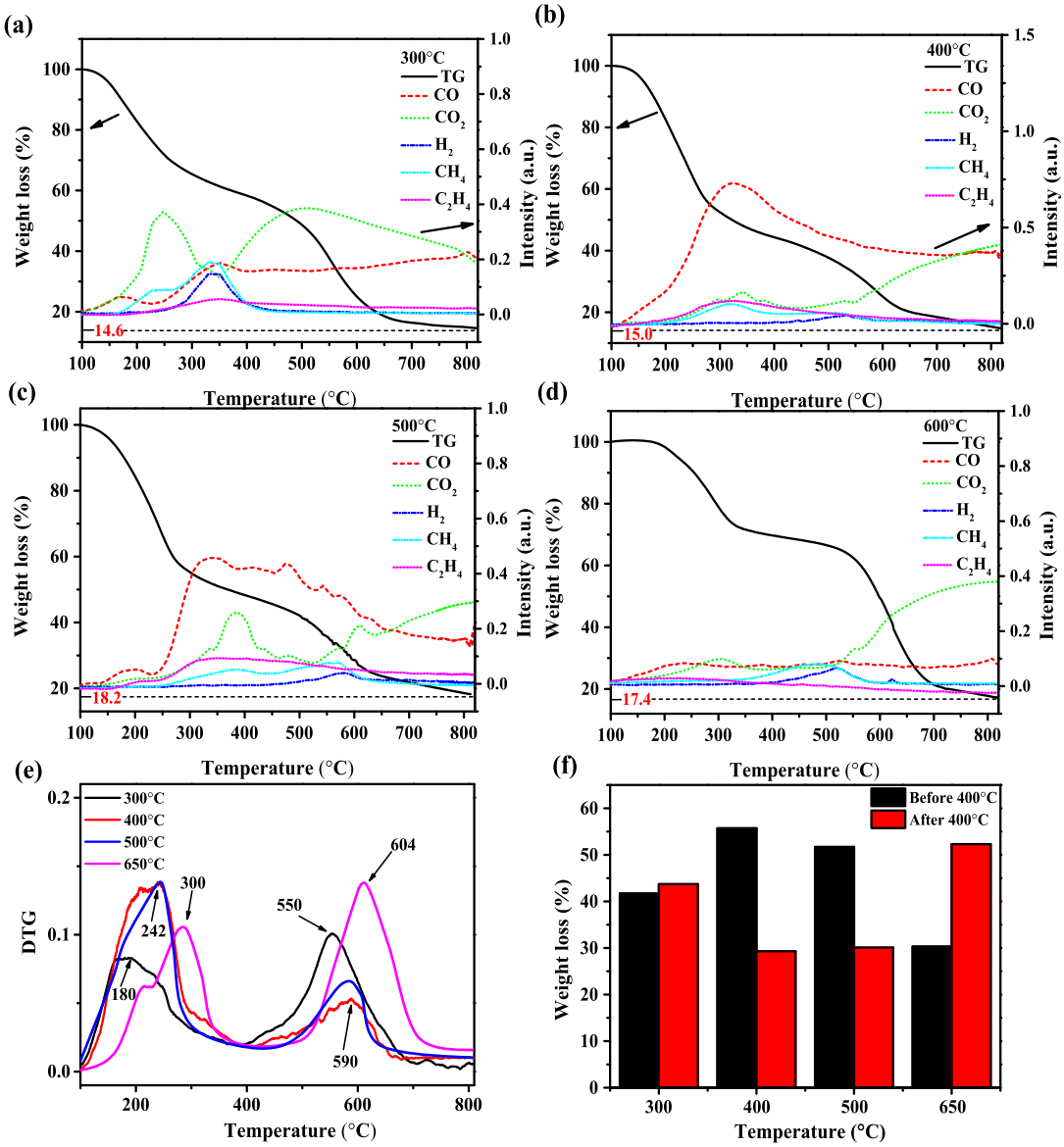

Fig. 6. Thermogravimetric characterization for the tar in the N_2 atmosphere and the changes of gas abundance during the TG tests with an in–situ MS (TG–MS): (a) 300 °C; (b) 400 °C; (c) 500 °C; (d) 650 °C; (e) DTG; (f) The Weight loss rate in each reaction temperature range.

in Fig. 6. The high pyrolysis temperature enhanced the thermal stability of the tar product. The percentage of the weight loss decreased from 85.4% at 300 °C to 81.8% at 500 °C, while at 650 °C, the weight loss percentage of tar rose a little to 82.6%. It was because the oxygen content of in the tar increased at the pyrolysis temperature above 550 °C, as previously indicated in Table 2. In addition, the DTG results also evidenced the increased thermal stability of the tar produced at the high pyrolysis temperatures (Fig. 6e). For the bio-oil produced at 300 °C, the two weight loss peaks appeared at 180 and 580 °C, respectively. As the pyrolysis temperature raised, the weight loss peaks shifted toward the high temperatures, indicating the improved thermal stability of the components in the tar produced at the high reaction temperatures. Based on the range of the two peaks in the DTG curves, the weight loss in the TG curves could be divided into two regions. The results in Fig. 6f showed that the light components were predominant at the medium pyrolysis temperatures. Interestingly, although the tar produced at 650 °C had lower carbon content while a higher oxygen content, the tar showed a higher thermal stability. The heavy components in the tar might be phenolics with multiple oxygen-containing functionalities and connected with ether bonds, leading to the higher oxygen content but also a higher thermal stability.

The relative abundance of the gaseous products during the TG characterization was shown in Fig. 6. CO, CO_2, H_2, CH_4 and C_2H_4 were the main gaseous products and their abundances were very different from the thermal treatment of the tar produced from the different pyrolysis temperatures. For the tar produced at 300 °C, CO and CO_2 were generated simultaneously, and the abundance of CO_2 was always higher than that of CO, which was formed probably in parallel. CO_2 could be formed from the decarboxylation reaction or the integration of *CO with a *O radical. In addition, the relatively higher intensity of the H_2 and CH_4 peaks indicated the abundant aliphatic structures in the tar produced at 300 °C. For the tar produced at 400 and 500 °C, CO was a more abundant product. The results of GC–MS also confirmed the formation of the phenolics with the carbonyl functionality (Fig. 3b). For the tar produced at 650 °C, except the formation of CO_2 at the elevated

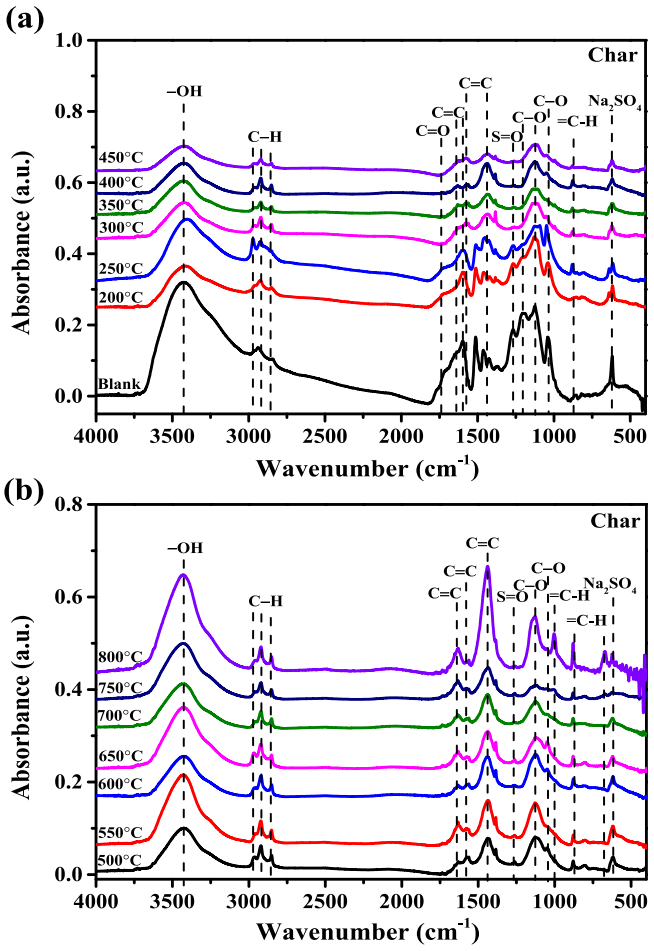

Fig. 7. FT–IR characterization of char from lignin pyrolysis at different recation temperature.

temperature, the formation of other gaseous products was negligible, further confirming the stable structure of the components in the tar produced at 650 °C.

3.6. Analysis of the char product

3.6.1. FT–IR characterization

The FT-IR spectra of lignin and the char generated at the different pyrolysis temperatures were shown in Fig. 7. The FT-IR spectrum of tar obtained below 250 °C showed some similarity to that of lignin. The absorption peaks of C═O, S═O and C—O were observed at 1740, 1260 and 1120 cm^{-1}, respectively, while the intensity decreased significantly versus the increasing pyrolysis temperature. This was caused by the removal of the sulfonic functionality, the cleavage of the ether bond connecting the structural unit, and the volatilization of the organic substance containing the carbonyl functional group. The C═C stretching vibration peaks of olefin located at 1640 and 1600 cm^{-1}, respectively. With the increase of the pyrolysis temperature, the intensity of the absorption peaks decreased. Correspondingly, the strength of the benzene-ring skeleton vibration peak at 1580 and 1440 cm^{-1} and the bending vibration peak of aromatic hydrocarbon at 680 cm^{-1} were enhanced. It proved that high pyrolysis temperature could promote the aromatization of char. The thermal stability of biochar and the gases released during the heating of biochar were further characterized with TG-MS.

3.6.2. TG-MS characterization of the char

Fig. 8 shows the TG-MS results for the characterization of lignin and the biochar. The thermal stability of the char was improved with the increase of the pyrolysis temperature, as evidenced by the gradually decreased mass loss. This was understandable as the higher pyrolysis temperature could remove more volatiles and produced the residual with the improved thermal stability. The remarkable weight loss could be separated into two stages, as evidenced in the DTG curves. The volatile component of lignin could be removed at the pyrolysis temperature of 400 °C while the heavy component of lignin could only decompose at ca. 750 °C. The thermal stability of the heavy component was inherent from lignin and not affected by the pre-treatment (pyrolysis) at the varied temperature. As evidenced in Fig. 8a and f, the char obtained at the different pyrolysis temperature showed the weight loss peak almost at exactly the same temperature of ca. 750 °C.

The abundance of the gases generated from the thermal treatment of lignin and the char was measured with an in situ MS. CO_2 was a major product accompanying with the significant weight loss at 750 °C, while other gases such as CO, CH_4 and H_2 were also observed, especially for the char produced at the low temperatures. They were formed from the volatile fraction of lignin. After the removal of the volatile fraction in lignin after the pyrolysis at 400 °C (Fig. 8g), CO and CH_4 formation were decreased while H_2 peak were observed in all the samples at ca. 600 °C. The release of H_2 was the sign for the fusion of the aromatic ring structures. The evolution of the functionalities of biochar was further investigated with DRIFTS study.

3.6.3. DRIFTS characterization of the char

Figs. 9 and 10 show the DRIFTS spectra of lignin feedstock or the char during the heating to 700 °C in vacuum. From 200 to 300 °C, the absorption of carbonyl functionality increased, indicating the occurrence of dehydration or other reactions that resulted in the formation of the functional group. From 300 to 400 °C, the distribution of the functional groups did not change significantly. Nevertheless, with the increase of the temperature to 500 °C, in addition to the C═O in ketones at 1680 cm^{-1}, the C═O in aldehydes at 1748 cm^{-1} were also formed. Further to this, the absorption peak for = C-H functionality also intensified, suggesting the enhancement of the formation of the unsaturated functionalities. The drastic changes of the absorption patterns took place at the temperature from 520 to 530 °C, as detailed in Fig. S4. With the increase of the temperature from 520 to 530 °C, within the scale 10 °C, the absorption of C═O peaks disappeared, while the absorption of C—H peaks were also substantially weakened. In the meantime, the intensity of absorption of C═C, C—O and =C—H was significantly increased. Clearly, a major change for the internal structure took place in this temperature range. The carbonyl functionality and the saturate —C—H (the aliphatic structure) were removed, and new π-bonds or conjugated π-bond systems were formed. The ether bond, which connected the benzene rings, was rather stable, and their absorption was still remarkable even at 700 °C. The lone electron pair in the oxygen of the ether bond could form n → π conjugation with the benzene ring, which enhances the dissociation energy the bonds.

For the char produced at the varied pyrolysis temperatures, the temperature for drastic change of the structure, which referred to the removal of carbonyl functionality and the aliphatic structure (saturate —C—H) was mainly in the range of 400–500 °C. During the pyrolysis, the cross-link structure of lignin could be destroyed or partially destroyed, so the temperature required for the cracking could decrease. In addition, the absorption of the hydroxyl group also decreased significantly from 400 to 500 °C, indicating the deoxygenation of the hydroxyl group in the phenolic structure unit. In addition, for the char obtained from pyrolysis above

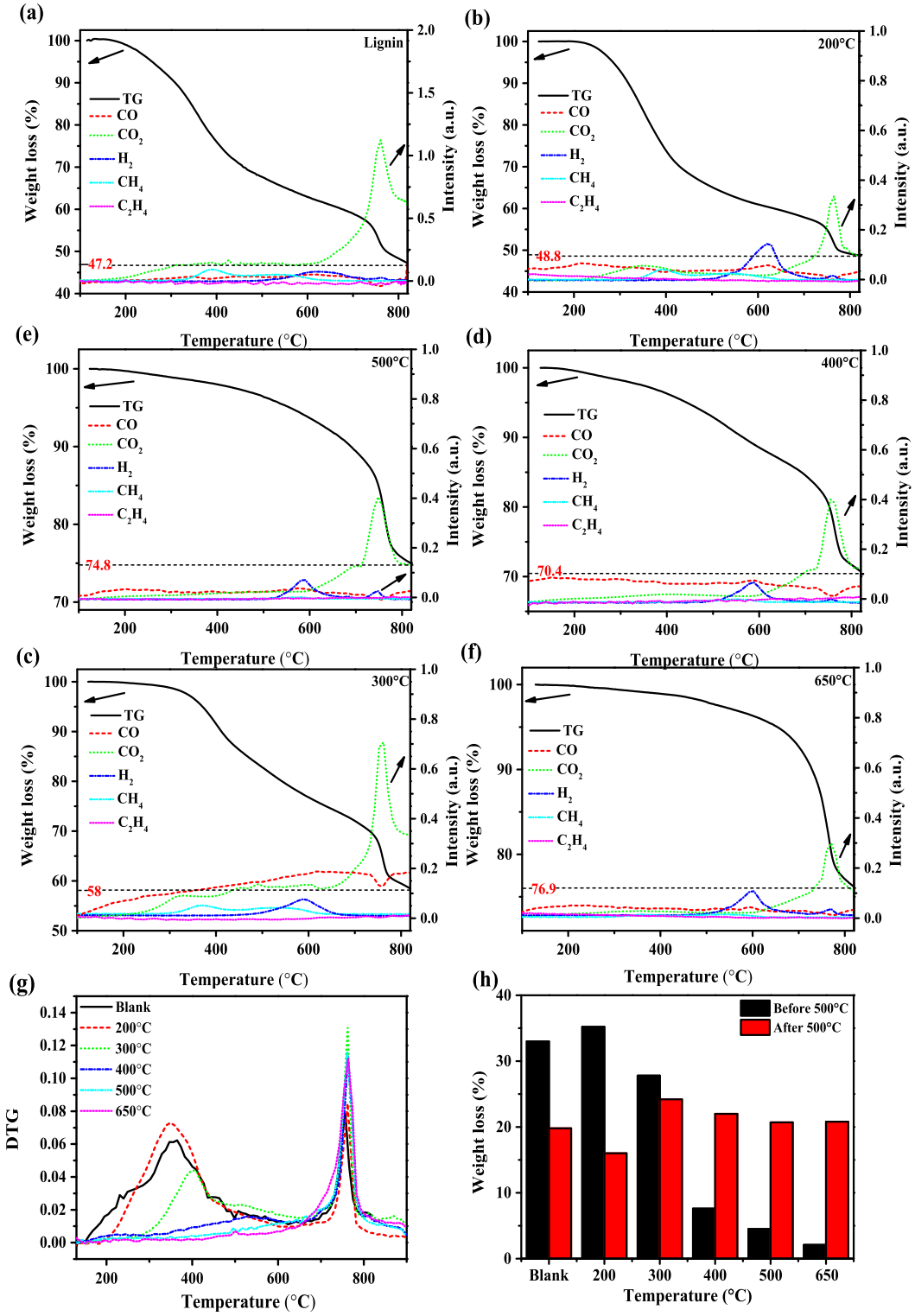

Fig. 8. Thermogravimetric characterization of the char in the N_2 atmosphere and the changes of gas abundance during the TG tests was dectect by MS: (a) lignin; (b) 200 °C; (c) 300 °C; (d) 400 °C; (e) 500 °C; (f) 650 °C; (g) DTG; (h) The weight loss rate.

400 °C, the intensity of C—H absorption peak around 3000 cm^{-1} decreased significantly, which was consistent with the TG-MS results that the char generated at high pyrolysis temperature had negligible alkane chains.

3.6.4. TPO–MS characterization of the char

The reactivity of char with oxygen was measured with TPO-MS and the results were given in Fig. 11. In a sufficient oxygen atmosphere, char was oxidized to form mainly CO_2. During the heating, the char formed at a pyrolysis temperature of 200 °C showed two oxidation peaks at 439 and 573 °C, and the latter oxidation peak was dominant. The main oxidation temperature of the main oxidation peak of char formed at a pyrolysis temperature of 400 or 500 °C was around 595 °C, indicating that the decreased volatility and the increased thermal stability of char produced at the high pyrolysis temperatures. Fig. S5 further indicated that oxidation

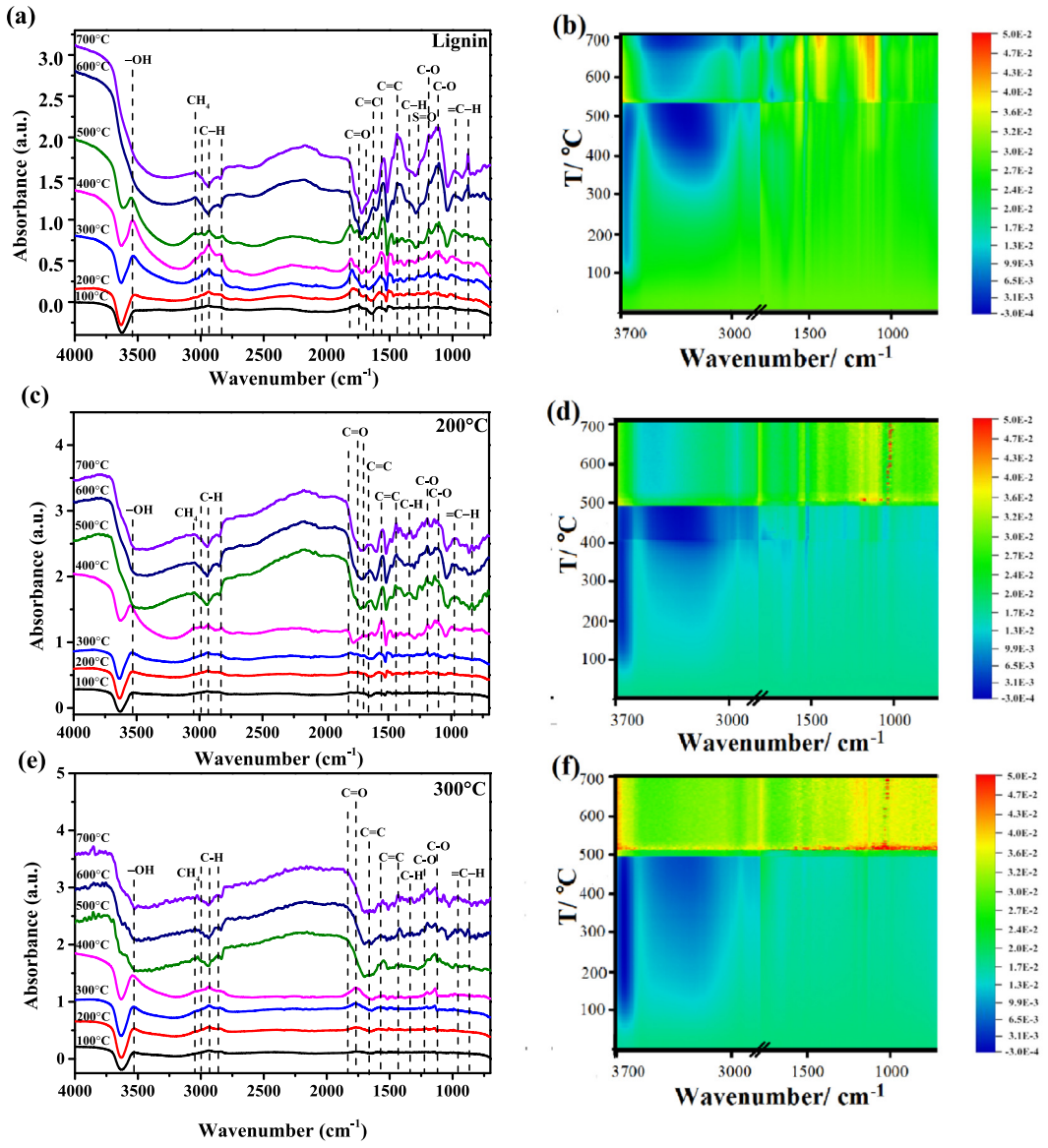

Fig. 9. DRIFTS characterization for the feedstock and char in the vacuum environment: (a, b) lignin; (c, d) 200 °C; (e, f) 300 °C.

peak of char obtained from lignin pyrolysis at 800 °C obviously moved to the high temperature zone. Furthermore, the oxygen consumption (the peak area) required for oxidation of the char also increased for the char produced at the high temperature, which was directly related to the increase in the percentage of carbon in the char. In addition to the reactivity of the char toward oxidation, the char structure was also explored by XRD and Raman characterizations.

3.6.5. XRD analysis of the char

The XRD patterns of the char produced at the different temperatures were shown in Fig. 12a and b. The XRD pattern of char generated at the pyrolysis temperature below 250 °C was similar to that of lignin. The alkali-depleted lignin contained disodium sulfate, diffraction of which was very significant. With the increase of the pyrolysis temperature, disodium sulfate still existed in the char, but its internal structure changed. The space group was changed from the original Fdd (70) to Cmm (63). After the pyrolysis temperature reaching 500 °C, the crystal structure of sodium sulfate changed from an orthorhombic structure to a hexagonal structure. As the pyrolysis temperature continued to increase, the half-peak width of disodium sulfate gradually decreased, and the peak height also increased. Above 700 °C, sodium sulfate began to decompose and its diffraction peak intensity began to decrease. In the TG-MS characterization of the char, the weight decreased significantly above 700 °C, which might be related to the decomposition of sodium sulfate. In addition, a broad peak at 10–30° and another one at 40–48° corresponded to the (002) lattice plane and the (100) lattice plane of turbostratic carbon crystallites (Yu et al., 2018). The appearance of these two wide peaks indicated that large diameter grains were formed in the char product. It was obvious that high pyrolysis temperature (above 700 °C) could promote the structure of char more orderly.

3.6.6. Raman characterizations of char

Raman spectra of the char generated at the different pyrolysis temperatures were given in Fig. 12c. The variation of the total area of Raman peak of char with the pyrolysis temperature was given in Fig. 12d. According to relevant literature reports, the enhanced aromatization of char leads to the correspondingly reduction of

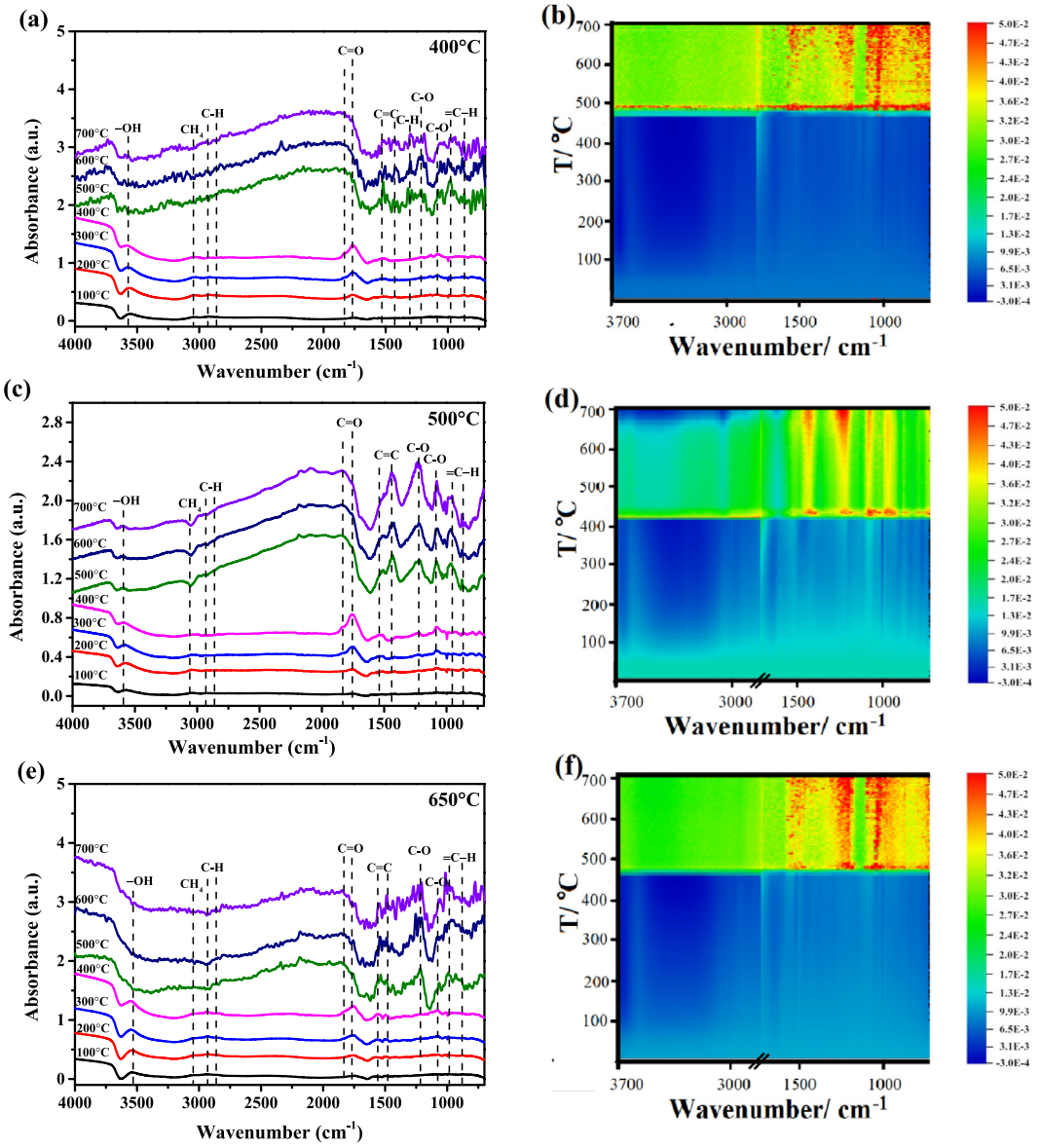

Fig. 10. DRIFTS characterization for the char in the vacuum environment: (a, b) 400 °C; (c, d) 500 °C; (e, f) 650 °C.

the total Raman area (Li et al., 2017; Chen et al., 2012). With the increasing pyrolysis temperature, the increase of the ratio of D/G band indicated the increase of the size of the aromatic ring structures with the conjugated π-bonds, which increased the absorption of the laser light and correspondingly decreased the total area of the Raman spectra. Although the C/H ratio of char decreased from 700 to 800 °C, the result of XRD characterization showed that crystal formation with stronger light absorption capacity. Therefore, the total Raman area reached the minimum at 800 °C.

Raman spectroscopy is usually used to study the structure of carbon materials and the ratio of D/G band is often used to indicate the degree of graphitization (Sun et al., 2019). However, char formed from pyrolysis of biomass at low temperatures is a disorder material and contains abundant aliphatic structures and oxygen-containing functionalities, which differs from that of ordered carbon materials (Yu et al., 2018). Furthermore, the size of the aromatic hydrocarbons contained in this type of char is far from the size required to form graphite crystals (Keiluweit et al., 2010). In addition, lignin has a highly crosslinked and three-dimensional structure, which was a barrier for graphitization (Sagues et al., 2019). Herein, the char generated below 700 °C with the very wide D band suggested that the char contained different size of aromatic rings, which, however, was not the graphite crystal (Li et al., 2006). The D band at around 1340 cm^{-1} represented the aromatic ring structure with more than 6 fused benzene rings with defects caused by stacking faults, crystallite size, or edge states (Asadullah et al., 2010). The G band at around 1590 cm^{-1} can be ascribed to aromatic ring breathing (Kim et al., 2011).

The ratio of D/G band at the varied pyrolysis temperature represented the evolution of aromatic hydrocarbon system in the char (Yang et al., 2016). As the pyrolysis temperature increased from 200 to 700 °C, the ratio of D/G band increased from 0.64 to 2.52. This indicated that aromatic hydrocarbons with less than 6 rings were transformed into the aromatic hydrocarbons with more than 6 rings, accompanied by an increase in defect structure (Guizani et al., 2017). According to the result of the elemental analysis (Table 1), the ratio of C/H increased monotonously with the increase of the pyrolysis temperature to 700 °C, indicating that the high pyrolysis temperature promoted the dehydrogenation, the further polymerization of the resulting char or the condensation among small aromatics

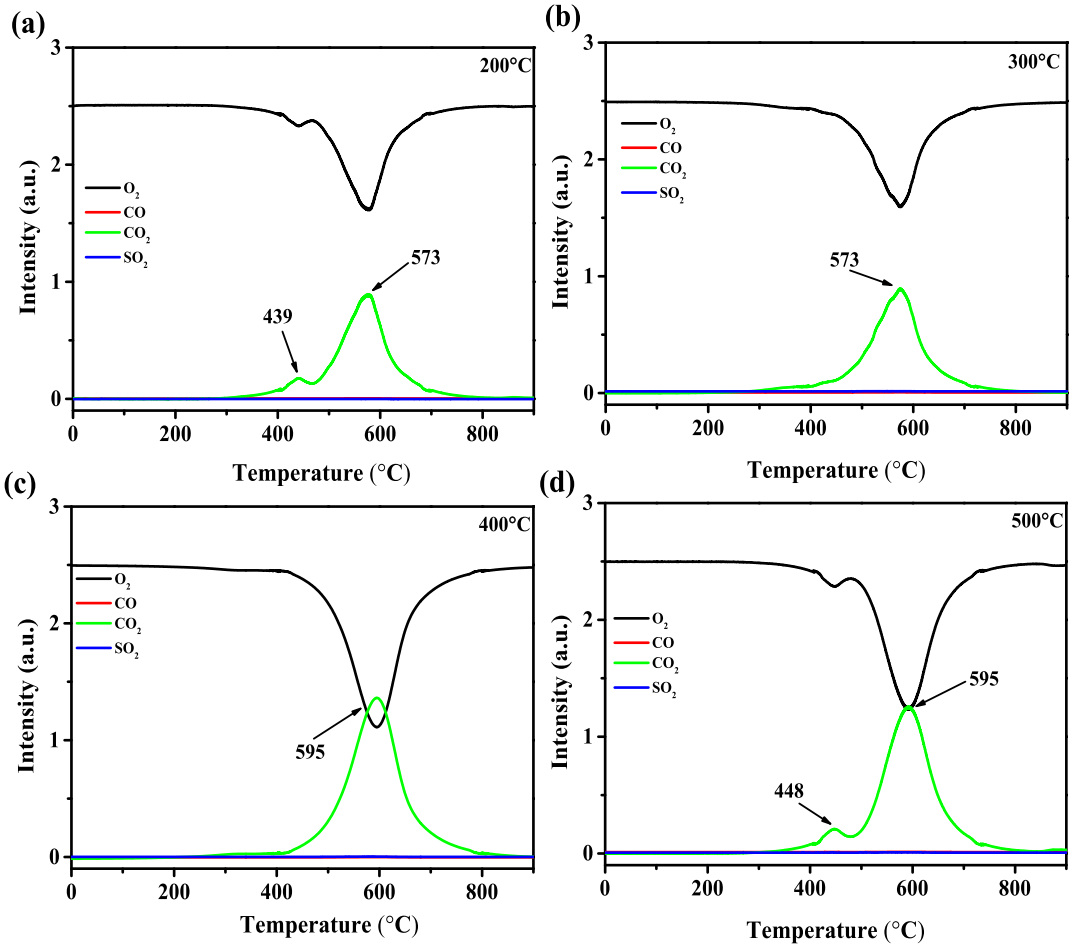

Fig. 11. TPO-MS characterization of the char from lignin pyrolysis at different temperature. (a) 200 °C; (b) 300 °C; (c) 400 °C; (d) 500 °C.

(Azargohar et al., 2014). The condensation of small aromatic rings into the large aromatic rings with the defective structure was the potential evolution path of the biochar structure versus the increasing pyrolysis temperature (Keiluweit et al., 2010). It was believed that, following the depolymerization of lignin, the further condensation of the aromatic hydrocarbons also occurred, leading to the increase of the ratio of D/G band (Sagues et al., 2019). In addition, the diffraction peaks of turbostratic carbon crystallites could be observed in the XRD pattern of the char generated at 800 °C. The fused benzene structure with more than 6 benzene rings in the char was probably further decomposed at this high temperature.

3.7. Pyrolysis mechanism of lignin

In order to explore the pyrolysis mechanism of lignin, the DRIFTS spectra of lignin feedstock that was heated from 100 to 700 °C in the N_2 atmosphere was conducted and the results were given in the Fig. S6. In the heating progress from 100 to 300 °C, the joint bonds, such as C—C bonds and C—O bonds, between the internal structural units of lignin were broken, forming more alkane chains and carbonyl groups. It was evidenced that a significant increase in the absorption of carbonyl peaks and alkanes peak at 1680–1810 cm^{-1} and 2830–3000 cm^{-1}, respectively. In addition, the absorption peak of —OH at 3550 cm^{-1} was strengthening, suggesting the formation of more phenolic structures during the pyrolysis of lignin. With the further increasing temperature, the absorption of the C═O peak at 1810 cm^{-1} represented the esters and the C═O in the aldehydes at 1748 cm^{-1} decreased remarkably, while the C═O in the ketone at 1680 cm^{-1} maintained the absorption intensity. This result indicated that the esters and aldehydes in lignin were removed by decarbonylation, while organic compounds with aldehyde groups had stable structures, resulting in the higher thermal stability. In the meantime, the intensity for the absorption peak of C═C at 1560 cm^{-1} was elevated, suggesting the acceleration of the aromatization or the fusion of the ring structures. When the increasing the pyrolysis temperature above 500 °C, the functional groups contained in lignin were further removed and the degree of carbonization was further improved. The relative absorption of —OH and C—H band decreased significantly, indicated that the phenolic and alkanes were decomposed at the high temperature. In addition, most carbonyl groups in the solid samples were completely removed and only a few carbonyl groups belonging to ketones existed. In the other hand, ether bonds also had the relatively higher thermal stability. The strong absorption of C═C and ═C—H bands evidenced the existence the most of carbon atoms in the form of aromatic hydrocarbons.

3.8. Kinetic parameters from pyrolysis of lignin and char

The DTG curves of lignin and the char produced from the lignin pyrolysis at 200 °C were shown in Figs. S7 and 13, respectively. In Fig. 13, the DTG curve of the char obtained at 200 °C indicated that pyrolysis of char occurred over a wide temperature range, from 190 °C to 700 °C. In addition, DTG curves obtained at the different heating rates all contained a main peak which was associated with primary pyrolysis. Although acromion peak also existed in DTG

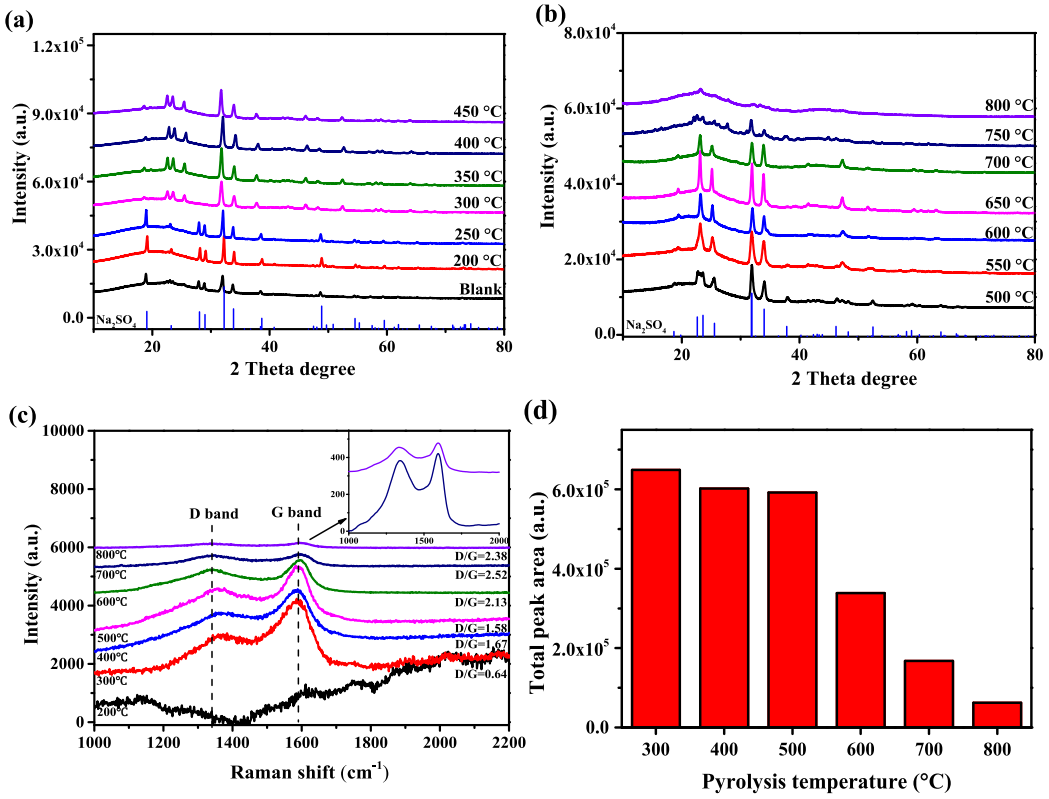

Fig. 12. XRD and FT-Raman characterization of the char from lignin pyrolysis at different reaction temperature. (a, b) XRD; (c, d) FT-Raman.

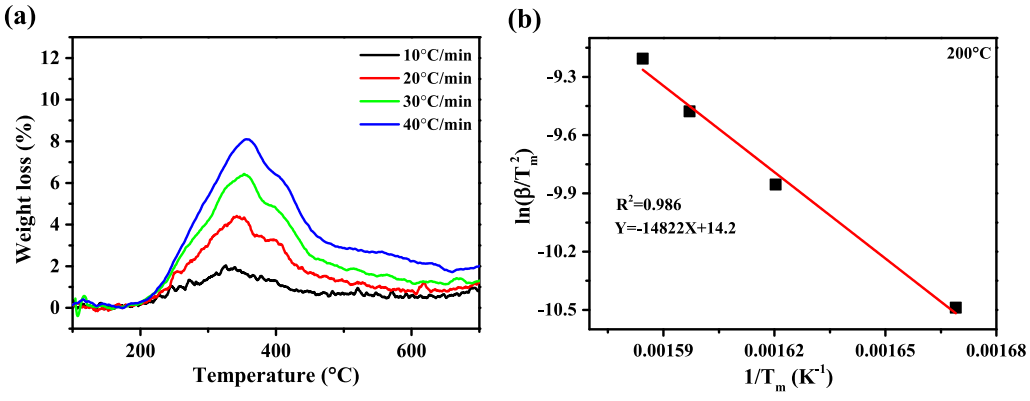

Fig. 13. (a) DTG cruve for the char from lignin pyrolysis at 200 °C. (b) Plot of $\ln(\beta/T_m^2)$ against $1/T_m$ for the char.

curve, it was much smaller than the main peak, so the main peak was used to calculate the kinetic parameters (Yeo et al., 2017). With the increasing heating rate, the main peak toward shifted upwards from 326.6 to 358.7 °C. The Kissinger's method was used herein to calculate the kinetic parameters by these temperatures corresponding to the top of the main peaks. The correlation coefficient between the calculated results and the experimental results was high. The R^2 value reached 0.986, indicating the credibility of the Kissinger's method.

The kinetic parameters from the pyrolysis of lignin and char obtained at 200 °C were summarized in Table 3. The pyrolysis activation energy of lignin and char was 204.7 and 123.3 kJ/mol, respectively. As char was the product of lignin pyrolysis at 200 °C, its internal structure had been changed by the heat, and some bonds had been broken, leading to the reduction of activation energy. Although the heating rate was different for the pyrolysis of lignin and char, the shape indexes (S) were similar. There was no relationship between order of reaction (n) and heating rate (Britt et al., 2000). Nevertheless, for the pyrolysis of lignin and char, they had different reaction order. This is because the pyrolysis of lignin proceeds in form of free-radical (Jiang et al., 2010b). The bigger reaction order meant the pyrolysis of lignin tended to generate smaller free radical compared with the pyrolysis of char (Bu et al., 2016). In addition, smaller free radicals are more likely to collide, resulting in an increase in the frequency factor. Therefore, the lignin had a larger frequency factor. Furthermore, compared with the char, the pyrolysis of lignin had higher activation energy. It was attributed the change of the internal structure of char after the reaction. The changes of the functionalities in the lignin at 200 °C have been described in the DRIFTS characterizations.

Table 3
Kinetic parameters at the different heating rates for the lignin and char pyrolysis.

Sample	β(°C/min)	S	T_{Max}(°C)	n	Kinetic parameters	
					E_α(kJ/mol)	A(min^{-1})
Lignin	10	0.82	333.4	1.14	204.7	2.7×10^{17}
	20	0.75	339.3	1.09		
	30	0.89	345.1	1.19		
	40	0.79	353.5	1.12		
Average		0.81	342.8	1.14		
200 °C	10	0.74	326.6	1.08	123.3	2.2×10^{10}
	20	0.71	344.3	1.06		
	30	0.67	353.4	1.03		
	40	0.75	358.7	1.09		
Average		0.72	345.8	1.07		

4. Conclusions

In summary, the results showed that reaction temperature showed significant impacts on distribution/properties of the products. Char was the main product during the pyrolysis of lignin with the pyrolysis temperature from 200 to 800 °C, but the structures changed drastically. The C/H ratio in the char was close to that in naphthalene (two fused rings) at 200 °C and was similar to that in anthracene (three rings) at 300 °C. The fusion of the ring structure accelerated at the further elevated temperature and was similar to pyrene (four fused rings) at 350 °C, and having 20 fused benzene rings at 550 °C. Growth of the fused aromatic ring structures continued with the further increase of pyrolysis temperature. The increasing pyrolysis temperature also shifted the products in the bio-oil from the phenolics to aromatic hydrocarbons, the oxygen-containing functionalities such as the carbonyl, esters, ketones functionalities to the ether bonds that had a higher thermal stability. The heavy components in bio-oil (tar) produced above 550 °C had a higher oxygen content but also a higher thermal stability, which were possibly the phenolics with the ring structures connecting with multiple ether bonds.

The DRIFTS study of pyrolysis of lignin showed that from 200 to 300 °C dehydration or other reactions took place, leading to the increased absorption of carbonyl functionality. The further increase of the temperature to 500 °C enhanced the formation of the unsaturated functionalities. Drastic changes of the functionalities and the internal structure occurred in a narrow temperature region from 520 to 530 °C. The carbonyl functionality and the saturate —C—H (the aliphatic structure) were removed, and new π-bonds or conjugated π-bond systems were formed. The ether bond, which connected the benzene rings, was rather stable. Further increase of reaction temperature led to the further aromatization of the char structure. In addition, after the reaction at 200 °C, the activation energy of generated char compared with raw material was greatly reduced. Pyrolysis temperature substantially impacted the structure of the resulting char, which should be taken into consideration during the further application of the lignin-derived char.

Declaration of Competing Interest

The authors declare that there is no conflict of interest regarding the publication of this article.

Acknowledgements

This work was supported by the National Natural Science Foundation of China (No. 51876080), the Strategic International Scientific and Technological Innovation Cooperation Special Funds of National Key Research and Development Program of China (No. 2016YFE0204000), the Program for Taishan Scholar Project of Shandong Province, the Recruitment Program of Global Experts (Thousand Youth Talents Plan), the Natural Science Foundation of Shandong Province (ZR2017BB002) and the Key Research and Development Program of Shandong Province (2018GSF116014).

Appendix A. Supplementary data

Supplementary data to this article can be found online at https://doi.org/10.1016/j.scitotenv.2019.134381.

References

Abhishek, Sharma, Vishnu, Pareek, Zhang, D., 2015. Biomass pyrolysis—a review of modelling, process parameters and catalytic studies. Renew. Sust. Energ. Rev. 50, 1081–1096.
Anca-Couce, A., Berger, A., Zobel, N., 2014. How to determine consistent biomass pyrolysis kinetics in a parallel reaction scheme. Fuel 123, 230–240.
Asadullah, M., Zhang, S., Min, Z., Yimsiri, P., Li, C.Z., 2010. Effects of biomass char structure on its gasification reactivity. Bioresour. Technol. 101, 7935–7943.
Azargohar, R., Nanda, S., Kozinski, J.A., Dalai, A.K., Sutarto, R., 2014. Effects of temperature on the physicochemical characteristics of fast pyrolysis bio-chars derived from Canadian waste biomass. Fuel 125, 90–100.
Britt, P.F., Buchanan, A.C., Cooney, M.J., Martineau, D.R., 2000. Flash vacuum pyrolysis of methoxy-substituted lignin model compounds. J. Org. Chem. 65, 1376–1389.
Bu, Q., Lei, H., Qian, M., Yadavalli, G., 2016. A thermal behavior and kinetics study of the catalytic pyrolysis of lignin. RSC Adv. 6 (103), 100700–100707.
Buller, L.S., Ortega, E., Bergier, I., Mesa-Pérez, J.M., Salis, S.M., Luengo, C.A., 2015. Sustainability assessment of water hyacinth fast pyrolysis in the Upper Paraguay River basin, Brazil. Sci. Total Environ. 532, 281–291.
Chaiwat, W., Gunawan, R., Gholizadeh, M., Li, X., Lievens, C., Hu, X., Wang, Y., 2013. Upgrading of bio-oil into advanced biofuels and chemicals. Part II. Importance of holdup of heavy species during the hydrotreatment of bio-oil in a continuous packed-bed catalytic reactor. Fuel 112, 302–310.
Chan, Y.H., Cheah, K.W., How, B.S., Loy, A.C.M., Shahbaz, M., Singh, H.K.G., Kansha, Y., 2019. An overview of biomass thermochemical conversion technologies in Malaysia. Sci. Total Environ. 680, 105–123.
Chen, Y., Yang, H., Wang, X., Zhang, S., Chen, H., 2012. Biomass-based pyrolytic polygeneration system on cotton stalk pyrolysis: influence of temperature. Bioresour. Technol. 107, 411–418.
Chen, Z., Leng, E., Zhang, Y., Zheng, A., Peng, Y., Gong, X., Qiao, Y., 2018. Pyrolysis characteristics of tobacco stem after different solvent leaching treatments. J. Anal. Appl. Pyrol. 130, 350–357.
Chua, Y.W., Yu, Y., Wu, H., 2017. Thermal decomposition of pyrolytic lignin under inert conditions at low temperatures. Fuel 200, 70–75.
Collard, F.X., Blin, J., 2014. A review on pyrolysis of biomass constituents: mechanisms and composition of the products obtained from the conversion of cellulose, hemicelluloses and lignin. Renew. Sust. Energ. Rev. 38, 594–608.
Das, O., Sarmah, A.K., Bhattacharyya, D., 2015. Structure–mechanics property relationship of waste derived biochars. Sci. Total Environ. 538, 611–620.
Dhyani, V., Bhaskar, T., 2018. A comprehensive review on the pyrolysis of lignocellulosic biomass. Renew. Energ. 129, 695–716.
Gholizadeh, M., Gunawan, R., Hu, X., Mercader, F.M., Westerhof, R., Chaitwat, W., Li, C.Z., 2016. Effects of temperature on the hydrotreatment behaviour of pyrolysis bio-oil and coke formation in a continuous hydrotreatment reactor. Fuel Process. Technol. 148, 175–183.
Gholizadeh, M., Hu, X., Liu, Q., 2019. A mini review of the specialties of the bio-oils produced from pyrolysis of 20 different biomasses. Renew. Sust. Energ. Rev. 114, 109313.
Guizani, C., Haddad, K., Limousy, L., Jeguirim, M., 2017. New insights on the structural evolution of biomass char upon pyrolysis as revealed by the Raman spectroscopy and elemental analysis. Carbon 119, 519–521.

Gunawan, R., Li, X., Lievens, C., Gholizadeh, M., Chaiwat, W., Hu, X., Li, C.Z., 2013. Upgrading of bio-oil into advanced biofuels and chemicals. Part I. Transformation of GC-detectable light species during the hydrotreatment of bio-oil using Pd/C catalyst. Fuel 111, 709–717.
Ha, J.M., Hwang, K.R., Kim, Y.M., Jae, J., Kim, K.H., Lee, H.W., Park, Y.K., 2019. Recent progress in the thermal and catalytic conversion of lignin. Renew. Sust. Energ. Rev. 111, 422–441.
Han, Y., Gholizadeh, M., Tran, C.C., Kaliaguine, S., Li, C.Z., Olarte, M., Garcia-Perez, M., 2019. Hydrotreatment of pyrolysis bio-oil: a review. Fuel Process. Technol. 195, 106140.
Hoslett, J., Ghazal, H., Ahmad, D., Jouhara, H., 2019. Removal of copper ions from aqueous solution using low temperature biochar derived from the pyrolysis of municipal solid waste. Sci. Total Environ. 673, 777–789.
Hu, X., Gholizadeh, M., 2019. Biomass pyrolysis: a review of the process development and challenges from initial researches up to the commercialisation stage. J. Energy Chem. 39, 109–143.
Iliopoulou, E.F., Stefanidis, S., Kalogiannis, K., Psarras, A.C., Delimitis, A., Triantafyllidis, K.S., Lappas, A.A., 2014. Pilot-scale validation of Co-ZSM-5 catalyst performance in the catalytic upgrading of biomass pyrolysis vapours. Green Chem. 16 (2), 2–674.
Jiang, G., Nowakowski, D.J., Bridgwater, A.V., 2010a. Effect of the temperature on the composition of lignin pyrolysis products. Energ. Fuel. 24 (8), 4470–4475.
Jiang, G., Nowakowski, D.J., Bridgwater, A.V., 2010b. A systematic study of the kinetics of lignin pyrolysis. Thermochimi. Acta. 498 (1–2), 61–66.
Jiang, Z., Liu, Z., Fei, B., Cai, Z., Yu, Y., 2012. The pyrolysis characteristics of moso bamboo. J. Anal. Appl. Pyrol. 94, 48–52.
Jiang, S., Hu, X., Xia, D., Li, C.Z., 2016. Formation of aromatic ring structures during the thermal treatment of mallee wood cylinders at low temperature. Appl. Energ. 183, 542–551.
José, M., Sánchez-Martín, Á.M., Campos, P., Miller, A.Z., 2019. Effect of pyrolysis conditions on the total contents of polycyclic aromatic hydrocarbons in biochars produced from organic residues: assessment of their hazard potential. Sci. Total Environ. 667, 578–585.
Kan, T., Vladimir, Strezov, Evans, Tim J., 2016. Lignocellulosic biomass pyrolysis: a review of product properties and effects of pyrolysis parameters. Renew. Sust. Energ. Rev. 57, 1126–1140.
Keiluweit, M., Nico, P.S., Johnson, M.G., Kleber, M., 2010. Dynamic molecular structure of plant biomass-derived black carbon (biochar). Environ. Sci. Technol. 44, 1247–1253.
Kim, P., Johnson, A., Edmunds, C.W., Radosevich, M., Vogt, F., Rials, T.G., Labbé, N., 2011. Surface functionality and carbon structures in lignocellulosic-derived biochars produced by fast pyrolysis. Energ. Fuel. 25 (10), 4693–4703.
Kim, T.S., Kim, J.Y., Kim, K.H., Lee, S., Choi, D., Choi, I.G., Choi, J.W., 2012. The effect of storage duration on bio-oil properties. J. Anal. Appl. Pyrol. 95, 118–125.
Kissinger, H.E., 1957. Reaction kinetics in differential thermal analysis. Anal. Chem. 29 (11), 1702–1706.
Li, X., Hayashi, J.I., Li, C.Z., 2006. FT-Raman spectroscopic study of the evolution of char structure during the pyrolysis of a Victorian brown coal. Fuel 85 (12–13), 1700–1707.
Li, T., Zhang, L., Dong, L., Zhang, S., Qiu, P., Wang, S., Li, C.Z., 2017. Effects of gasification temperature and atmosphere on char structural evolution and AAEM retention during the gasification of Loy Yang brown coal. Fuel Process. Technol. 159, 48–54.
Lievens, C., Mourant, D., He, M., Gunawan, R., Li, X., Li, C.Z., 2011. An FT-IR spectroscopic study of carbonyl functionalities in bio-oils. Fuel 90 (11), 3417–3423.
Lu, R., Sheng, G.P., Hu, Y.Y., Zheng, P., Jiang, H., Tang, Y., Yu, H.Q., 2011. Fractional characterization of a bio-oil derived from rice husk. Biomass Bioenergy 35 (1), 671–678.
Ma, Z., Yang, Y., Wu, Y., Xu, J., Peng, H., Liu, X., Wang, S., 2019. In-depth comparison of the physicochemical characteristics of bio-char derived from biomass pseudo components: hemicellulose, cellulose, and lignin. J. Anal. Appl. Pyrol. 140, 195–204.
Rover, M.R., Brown, R.C., 2013. Quantification of total phenols in bio-oil using the Folin–Ciocalteu method. J. Anal. Appl. Pyrol. 104, 366–371.
Sagues, W.J., Jain, A., Brown, D., Aggarwal, S., Suarez, A., Kollman, M., Park, S., Argyropoulos, D.S., 2019. Are lignin-derived carbon fibers graphitic enough? Green Chem. 21, 4253.
Sharma, R.K., Wooten, J.B., Baliga, V.L., Lin, X., Chan, W.G., Hajaligol, M.R., 2004. Characterization of chars from pyrolysis of lignin. Fuel 83 (11–12), 1469–1482.
Shen, Y., Zhao, P., Shao, Q., Ma, D., Takahashi, F., Yoshikawa, K., 2014. In-situ catalytic conversion of tar using rice husk char-supported nickel-iron catalysts for biomass pyrolysis/gasification. Appl. Catal. B-Environ. 152, 140–151.
Shuping, Z., Yulong, W., Mingde, Y., Chun, L., Junmao, T., 2010. Pyrolysis characteristics and kinetics of the marine microalgae Dunaliella tertiolecta using thermogravimetric analyzer. Bioresour. Technol. 101 (1), 359–365.
Stefanidis, S.D., Kalogiannis, K.G., Iliopoulou, E.F., Michailof, C.M., Pilavachi, P.A., Lappas, A.A., 2014. A study of lignocellulosic biomass pyrolysis via the pyrolysis of cellulose, hemicellulose and lignin. J. Anal. Appl. Pyrol. 105, 143–150.
Sun, Y., Iris, K.M., Tsang, D.C., Cao, X., Lin, D., Wang, L., Graham, N.J.D., Alessi, D.S., Komárek, M., Ok, Y.S., Feng, Y., Li, X.D., 2019. Multifunctional iron-biochar composites for the removal of potentially toxic elements, inherent cations, and hetero-chloride from hydraulic fracturing wastewater. Environ. Int. 124, 521–532.
Wang, Y., Hu, X., Mourant, D., Song, Y., Zhang, L., Lievens, C., Li, C.Z., 2013. Evolution of aromatic structures during the reforming of bio-oil: importance of the interactions among bio-oil components. Fuel 111, 805–812.
Wang, S., Dai, G., Yang, H., Luo, Z., 2017. Lignocellulosic biomass pyrolysis mechanism: a state-of-the-art review. Prog. Energ. Combust. 62, 33–86.
Xiao, R., Yang, W., 2013. Influence of temperature on organic structure of biomass pyrolysis products. Renew. Energ. 50, 136–141.
Xiong, X., Iris, K.M., Cao, L., Tsang, D.C., Zhang, S., Ok, Y.S., 2017. A review of biochar-based catalysts for chemical synthesis, biofuel production, and pollution control. Bioresour. Technol. 246, 254–270.
Xiong, Z., Wang, Y., Syed-Hassan, S.S.A., Hu, X., Han, H., Su, S., Hu, S., 2018. Effects of heating rate on the evolution of bio-oil during its pyrolysis. Energ. Convers. Manage. 163, 420–427.
Yang, H., Huan, B., Chen, Y., Gao, Y., Li, J., Chen, H., 2016. Biomass-based pyrolytic polygeneration system for bamboo industry waste: evolution of the char structure and the pyrolysis mechanism. Energ. Fuel. 30 (8), 6430–6439.
Yeo, J.Y., Chin, B.L.F., Tan, J.K., Loh, Y.S., 2017. Comparative studies on the pyrolysis of cellulose, hemicellulose, and lignin based on combined kinetics. J. Energy Inst. 92 (1), 27–37.
Yin, S., Dolan, R., Harris, M., Tan, Z., 2010. Subcritical hydrothermal liquefaction of cattle manure to bio-oil: effects of conversion parameters on bio-oil yield and characterization of bio-oil. Bioresour. Technol. 101 (10), 3657–3664.
Yu, J., Sun, L., Berrueco, C., Fidalgo, B., Paterson, N., Millan, M., 2018. Influence of temperature and particle size on structural characteristics of chars from Beechwood pyrolysis. J. Anal. Appl. Pyrol. 130, 127–134.
Zhang, C., Hu, X., Guo, H., Wei, T., Dong, D., Hu, G., Wang, Y., 2018. Pyrolysis of poplar, cellulose and lignin: effects of acidity and alkalinity of the metal oxide catalysts. J. Anal. Appl. Pyrol. 134, 590–605.
Zhao, C., Chen, A., Jiang, E., Qin, L., 2017. Pyrolysis of industrial waste lignin: analysis of product yields and character. Energ. Source. Part A. 39 (5), 458–464.
Zhao, B., O'Connor, D., Zhang, J., Peng, T., Shen, Z., Tsang, D.C., Hou, D., 2018. Effect of pyrolysis temperature, heating rate, and residence time on rapeseed stem derived biochar. J. Clean. Prod. 174, 977–987.